Available online at www.sciencedirect.com

ScienceDirect

journal homepage: www.elsevier.com/locate/he

Addition of transition metals to lithium intercalated fullerides enhances hydrogen storage properties

Matteo Aramini [a], Chiara Milanese [b], Daniele Pontiroli [a], Mattia Gaboardi [a], Alessandro Girella [b], Giovanni Bertoni [c,d], Mauro Riccò [a,*]

[a] Dipartimento di Fisica e Scienze della Terra, Università degli studi di Parma, Via G.Usberti 7/a, 43124 Parma, Italy
[b] Pavia H_2 Lab, C.S.G.I & Dipartimento di Chimica, Sezione di Chimica Fisica, Università degli Studi di Pavia, V.le Taramelli 16, 27100 Pavia, Italy
[c] IMEM-CNR, Parco Area delle Scienze 37/A, 43124 Parma, Italy
[d] Nanochemistry Department, Istituto Italiano di Tecnologia, via Morego 30, 16163 Genova, Italy

ARTICLE INFO

Article history:
Received 19 September 2013
Received in revised form
15 November 2013
Accepted 20 November 2013
Available online 25 December 2013

Keywords:
Hydrogen storage
Lithium fulleride
Transition metal decoration

ABSTRACT

We report an innovative synthetic strategy based on the solid state reaction of fullerene C_{60} with lithium-transition metals alloys (platinum and palladium), which provides transition metal-decorated lithium intercalated fullerides, with improved hydrogen storage properties. Compounds with $Li_6Pt_{0.11}C_{60}$ and $Li_6Pd_{0.07}C_{60}$ stoichiometry were obtained and investigated with manometric/calorimetric techniques which showed an 18% increase of the final H_2 absorbed amount with respect to pure Li_6C_{60} (5.9 wt% H_2) and an improved absorption process kinetic. The absorption mechanism was investigated with X-rays diffraction which allowed to identify the formation of the hydrofullerides. Scanning Electron Microscopy was applied to gain information on transition metal distribution and detected the presence of platinum and palladium aggregates which are shown to perform a surface catalytic activity towards hydrogen molecule dissociation process.

1. Introduction

Hydrogen is a promising energy vector due to its highest energy density if compared with other fuels but it still faces difficulties in automotive applications, mainly due to storage problems [1]. Since hydrogen density is often higher in solid materials than either its liquid and compressed gas phases, nowadays the interest is mainly focussed on the solid-state storage, which however still show strong limits, especially in terms of kinetics and reversibility.

One of the most important parameters driving the hydrogen sorption in bulk, solid materials is hydrogen binding energy (BE). Two extremes cases can be identified: *physical absorption* of the hydrogen molecule on a substrate, which is driven by relatively weak Van der Waals forces, whose energy is around few kJ/mol, and *chemical absorption* of atomic hydrogen, involving the break of the H_2 molecule and the formation of covalent bonds, whose energy is typically around hundreds kJ/mol. The BE in the former process is too low to yield useful gas storage at room temperature while, in the

* *Corresponding author*. Tel.: +39 0521905217; fax: +39 0521905223.
E-mail address: Mauro.ricco@fis.unipr.it (M. Riccò).
0360-3199/$ – see front matter
http://dx.doi.org/10.1016/j.ijhydene.2013.11.087

latter, the energy value is too high to be exploited for practical scopes. US-DoE [2] fixed in 20–50 kJ/mol a suitable value for room temperature application energy range.

Among the several investigated materials, carbon nanostructures are promising systems for hydrogen storage [3–5], since they are lightweight, can possess high surface/volume ratio and are relatively inexpensive. Theoretical investigation indicated that the storage capacity in carbon materials can be improved either by lowering the chemical absorption interaction energy (as usually happens in metal hydrides [6]) or by strengthening the physical absorption phenomena: examples of these two possibilities are based on the addition of metal clusters to the storage materials leading to the promotion of the so-called spillover effects [7]; alternatively, the presence of metal atoms decorating carbon layers was predicted to improve the hydrogen molecule binding by quantum mechanical mixing of the H_2 and metal orbitals (Kubas interaction) [8]. Theoretical studies have shown that metal-decorated fullerides, namely Na_8C_{60} [9] and $Li_{12}C_{60}$ [10], may absorb up to 9.5 and 13.5 wt% H_2 respectively.

Recent experimental works [11,12] tried to confirm these theoretical predictions and explored lithium and sodium intercalated fullerides, proving that Li_6C_{60} and $Na_{10}C_{60}$ are able to reversibly absorb up to 5 wt% and 3.5 wt% H_2 through the formation of a hydrogenated fullerene phase (so called "fullerane") at temperatures useful for applications. Similarly, also $Li_{12}C_{60}$ is able to absorb ~4.5 wt% H_2 at 225 °C (5 wt% at 350 °C), with the onset of hydrogenation below 100 °C [13]. The lowering of the hydrogenation temperature, together with the reversible character of the hydrogenation of the fullerene molecule, if compared with the hydrogenation process of bare C_{60}, can be explained admitting a key role played by the charge state of C_{60} molecules and by the presence of the alkali metal clusters intercalated in these compounds. Muon Spin Relaxation (μSR) measurement recently performed on Li_6C_{60} and $Na_{10}C_{60}$ fullerides [14] demonstrated that the atomic hydrogen absorption over charged fullerene can be even favored at cryogenic temperatures. Intercalated fullerides hydrogenation takes place in two steps: the H_2 molecule dissociation operated by intercalated alkali metal clusters and the subsequent hydrogen atoms absorption on C_{60}^{n-} molecules. The high temperatures usually necessary for the absorption in these materials are only required for the metal cluster assisted hydrogen molecule dissociation, limiting the hydrogenation process at still relatively high temperature.

In this scenario, the insertion of a transition metal able to promote hydrogen dissociation (i.e. platinum [15] or palladium) is expected to decrease the thermal energy required for H_2 dissociation and driving the material uptake properties to higher stored values. As a matter of facts, an increase in the H_2 uptake is highly desirable in order to make fullerides suitable for mobile application since they still do not meet US-DoE targets.

In the present paper we describe the insertion of platinum and palladium in lithium intercalated fullerides. We adopted a two step preparation: 1) high temperature synthesis of the Metal-Li alloy and 2) solid state high energy ball milling of the alloy and C_{60}. Scanning electron microscopy (SEM) and X-Ray powder diffraction (XRD) allowed a morphological and structural study focused on the phase evolution after hydrogenation while manometric and DSC characterization are presented to evaluate absorption properties in terms of stored hydrogen amount and sorption kinetics.

2. Experimental

Platinum (Sigma Aldrich, 99.99%) or palladium (Sigma Aldrich, 99.98%) were added to lithium metal (Sigma Aldrich, 99%) and placed together on a tantalum crucible into a Pyrex® vial which was sealed under 1 mbar He atmosphere. The two different mixtures (65–35 wt% of Li–Pt and 85–15 wt% of Li–Pd metals respectively, in the two alloys) were selected in order to prepare intermetallic compounds according to Li–Pt and Li–Pd phase diagrams [16].

Sealed vials were heated in a furnace at 400 °C and the temperature was kept stable for two hours. Samples were then removed from the oven and slowly cooled down to room temperature. X-rays diffraction (results not shown) excluded the segregation of either lithium or transition metals single phases therefore confirming the formation of alloys that were used as starting materials. Alloys were used as reagents for $Li_6Pt_{0.11}C_{60}$ and $Li_6Pd_{0.07}C_{60}$ solid state preparation: a stoichiometric amount of the alloys (either Li–Pt or Li–Pd) was cut in small pieces (around 1 mm each) and mixed to C_{60} powder (MER, 99.9% further purified with vacuum treatment at 250 °C for 12 h) in agate ball milling jar (5 ml volume with 3 agate of 10 mm diameter spheres were used) for a total amount of approximately 500 mg each sample.

Powders were mixed with 30 Hz frequency high energy ball milling in a Fritsch Mini-Mill Pulverisette23 for 30 min which were divided in 10 min turns, each separated by 5 min cooling. The air sensitivity of both $Li_6Pt_{0.11}C_{60}$ and $Li_6Pd_{0.07}C_{60}$ samples required their preparation and storage under strict oxygen and moisture free condition (Ar with less than 1 ppm O_2 and H_2O).

Hydrogenation studies were performed on the as prepared samples in the PCTPro-2000 manometric instrument by Setaram by heating them (about 200 mg each sample) from room temperature to 350 °C at 5 °C/min under 100 bar H_2 and appending an isotherm of 10 h. A portion of the discharged powders was analyzed by coupled calorimetric – manometric measurements by connecting the PCTPro to the Setaram Sensys high pressure DSC cells by stainless steel high pressure tubes. The charged powders (about 20 mg) were heated from room temperature up to 380 °C under 0.5 bar H_2 at 5 °C/min and the kinetic and calorimetric signals were recorded simultaneously. As a comparison, also a pure Li_6C_{60} sample was analyzed in the same conditions.

Scanning electron microscopy was performed on both the as prepared and the hydrogenated samples (without gold sputtering) by the Zeiss EVO®-MA10-HR microscope. To avoid air exposition of the samples, a home-made sample holder allowing the transfer of the samples from the glove-box in the SEM analysis chamber under vacuum has been used.

X-Ray powder diffraction analysis was performed by a Bruker D5005 diffractometer (Cu Kα radiation) in the angular range $2\theta = 5°–60°$ by using a suitable, sealed zero background sample holder allowing measurements under oxygen and moisture free Ar atmosphere.

For TEM analysis, a small amount of sample was exposed to air and dispersed in cyclohexane. The suspension was sonicated for a minute and a droplet was deposited onto ultrathin (~3 nm thick) carbon coated copper grid. High Angle Annular Dark Field (HAADF) Scanning Transmission Electron Microscopy (STEM) were carried out on a JEOL JEM-2200FS microscope with a Schottky gun working at 200 kV (STEM nominal probe size 0.5 nm), equipped with an in-column energy filter (Ω-type), a CCD high resolution camera and STEM detectors.

3. Results and discussion

3.1. Calorimetric – manometric measurements

Fig. 1 reports the kinetic curves of the pure Li_6C_{60} compound (a) compared with those of the Pt and Pd doped samples (b and c respectively). Clearly, all the samples absorb more than 5 wt %. The doped samples however reach a hydrogen charge value of 3 wt% and 4 wt% at 295 °C and 345 °C respectively, while for the pure sample the same hydrogen content is reached at 350 °C, during the isothermal stage. Moreover, the final gravimetric capacity is higher for the transition metal - doped samples with respect to the pure one (about 5.9 wt% vs 5.1 wt%).

Such an increase in the final uptake values with respect to Li_6C_{60} reflects an average stoichiometric hydrogen values $Li_6Pt_{0.11}C_{60}$–H_{47} and $Li_6Pd_{0.07}C_{60}$–H_{46} while in the pristine sample Li_6C_{60}–H_{40} is achieved [14].

Concerning kinetics, during the heating ramp the sorption rate is approximately $4.30 \cdot 10^{-2}$ wt%/min for the pure Li_6C_{60} compound, $5.55 \cdot 10^{-2}$ wt%/min for the Pt sample and up to $6.77 \cdot 10^{-2}$ wt%/min for the Pd containing one.

By the coupled manometric - DSC measurements (see Fig. 2), it is possible to conclude that the onset temperature for dehydrogenation decreases from 306 °C for the pure compound to 301 °C for the Pd containing sample down to 292 °C for the Pt one. On the contrary, the related dehydrogenation enthalpy values seems to increase a little, from 63 kJ/mol H_2 for the pure sample to 66 kJ/mol for the Pd one.

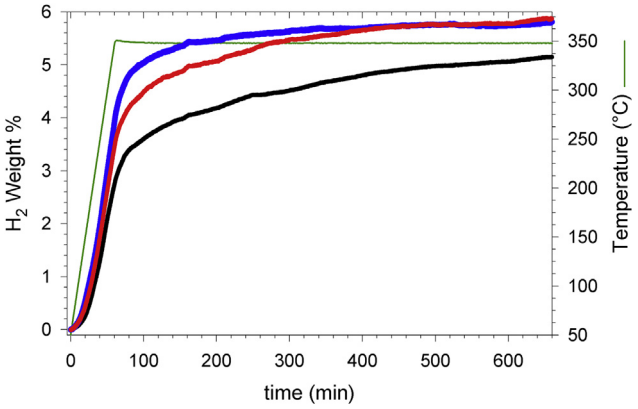

Fig. 1 – Kinetic absorption curves for the Li_6C_{60} sample (black, bottom line), for the Pt decorated sample (red, middle line) and for the Pd containing one (blue, top line). The temperature ramp profile is also reported (green thin line). (For interpretation of the references to color in this figure legend, the reader is referred to the web version of this article.)

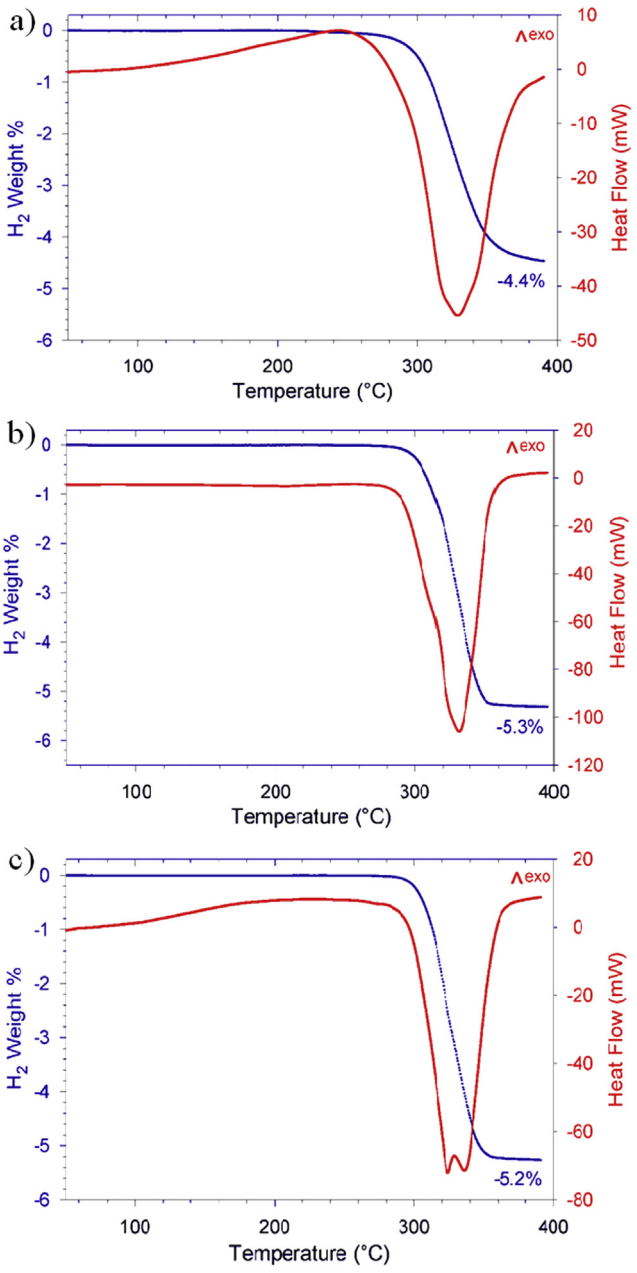

Fig. 2 – Coupled manometric–calorimetric desorption profiles for the bare Li_6C_{60} (a) and the doped samples $Li_6Pt_{0.11}C_{60}$ (b) and $Li_6Pd_{0.07}C_{60}$ (c).

3.2. X-rays diffraction

X-ray diffraction performed on as-prepared $Li_6Pt_{0.11}C_{60}$ (lower panel in Fig. 3) shows the presence of the majority phase Li_6C_{60}, accounting for the most intense peaks in the range $2\theta = 10$–$40°$. Peaks of this phase appear broad, but they can be

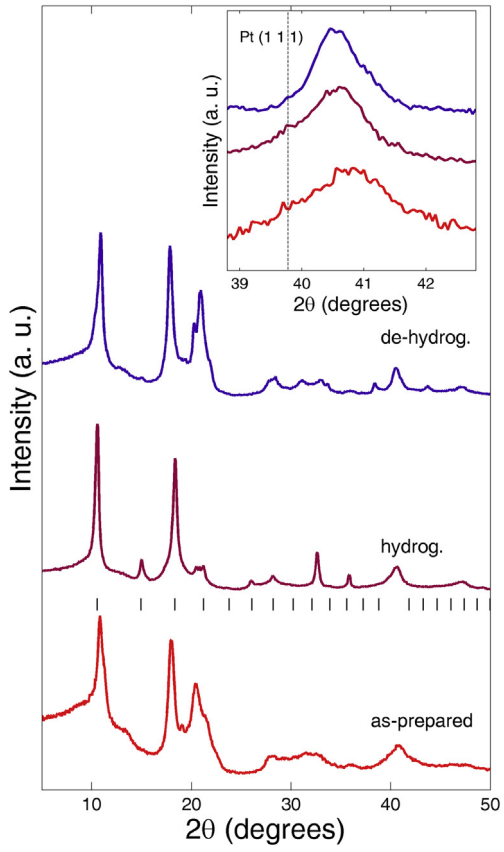

Fig. 3 – X-ray diffraction profiles of $Li_6Pt_{0.11}C_{60}$ collected on the as-prepared sample (lower, red line), on the sample after hydrogenation (intermediate, purple line) and after de-hydrogenation (top, blue line). The black ticks mark the reflection positions of the hydrofullerite $C_{60}H_{36}$ in H-treated sample, accordingly to [20] *Inset*: magnification of diffractograms around expected Pt(111) peak reflection at $2\theta = 40.7°$. The dashed line indicates the expected position for the (1 1 1) reflection of Pt. (For interpretation of the references to color in this figure legend, the reader is referred to the web version of this article.)

easily indexed with an *fcc* monomer phase belonging to the lithium intercalated fulleride plus a monoclinic cell isostructural to Li_4C_{60} polymer, accordingly to [17].

At higher angles, two broad reflections, respectively at $2\theta = 40.7°$ and $2\theta = 47.4°$, witness the presence of Pt particles, which segregates during the synthesis procedure. The expected position for the reflection (1 1 1) of Pt is however at $2\theta = 39.8°$ [18] and the rather large upshift of this reflection is not yet completely understood, although the strong reduction of the size of the particles (see below) could account for a sensitive contraction of the Pt cell dimension.

A crude estimation of the particle size can be obtained from the broadening of the X-ray reflection by the Scherrer's formula $p = K\lambda/b \cos\vartheta$, where p is the size of the crystallite (defined as the cube root of the volume of particle), b is the width of the peak, θ is the Bragg angle and K is the Scherrer constant that was taken 0.90 in this case, as originally proposed by Scherrer [19]. The fit of the (111) peak gives an average diameter of ~4 nm, a value much smaller as compared with the dimensions of Pt clusters captured in the SEM images (see next paragraph). This suggests that the metal aggregates visible by SEM are composed of very small crystallites.

After the treatment under hydrogen at high temperature (intermediate diffractogram in Fig. 3), the majority of the sample takes a *bcc* crystalline arrangement (a = 11. 83(3) Å). The same structure was observed in the hydrofullerene $C_{60}H_{36}$ [20]. The loss of the C_{60} I_h icosahedral symmetry in $C_{60}H_y$ molecules makes the *bcc* arrangement energetically favorable with respect to the *fcc*.

The peaks of metal Pt are still present in the hydrogenated sample (intermediate diffractogram in Fig. 3), while no PtH_x phases were observed. In this case (see Fig. 3, Inset) near the broad peak observed in the as-prepared sample, a new narrower peak is present, whose position is in very good agreement with Pt (1 1 1) reflection. This indicates that the high temperature reached during hydrogenation could induce a partial rearrangement of Pt nanoparticles.

Some small peaks of the diffractogram were indexed with the fcc cell of pristine C_{60} (S.G.: *Fm-3m*, a = 14.16 Å, see Fig. 4), corresponding to roughly 5 wt% in mass of the sample and indicating that the H treatment was not effective to hydrogenate the whole fullerene molecules. The transition from the polymer phase of lithium fulleride to its monomer *Fm-3m*

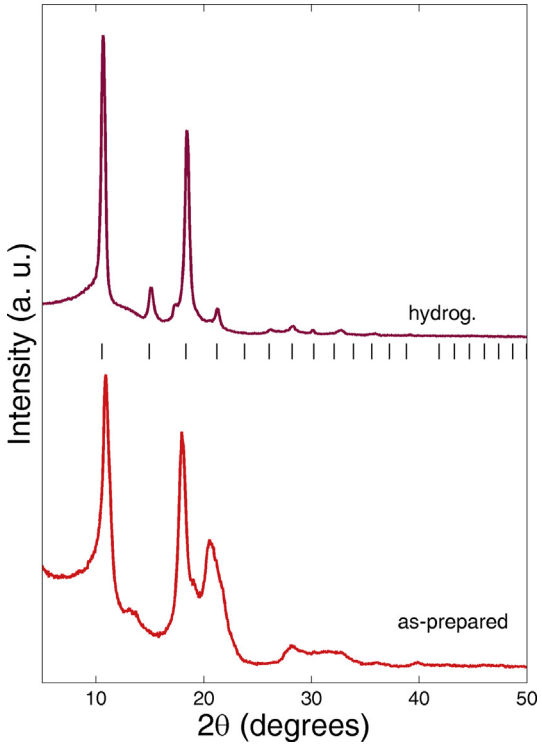

Fig. 4 – X-ray diffraction profiles of $Li_6Pd_{0.07}C_{60}$ collected on the as-prepared sample (red line) and on the sample after hydrogenation (purple line). The black ticks mark the reflection positions of the hydrofullerene $C_{60}H_{36}$ (see text). (For interpretation of the references to color in this figure legend, the reader is referred to the web version of this article.)

phase is known to take place [21] at the temperature reached during hydrogenation isotherm.

After the de-hydrogenation, the sample recovers the original structure with an increase in the monomer phase, confirming that the hydrogenation process of the fullerene molecules is reversible (see Fig. 3). After de-hydrogenation, the peak of metal Pt again appears upshifted and broader, indicating a clear structural activity of Pt in hydrogen absorption and desorption.

X-ray diffraction data collected on $Li_6Pd_{0.07}C_{60}$ indicate that in the as-prepared sample only the Li_6C_{60} phase is present, while no evident traces of Pd segregation are evident. After the hydrogen treatment, the crystalline structure changes and the peaks can be indexed with a *bcc* cell with $a = 11.81(6)$ Å, similarly to what observed in $Li_6Pt_{0.11}C_{60}H_y$. In this case, no spurious phases arising from metal hydrides segregation (LiH or PdH_x) or carbonaceous phases different from the hydrofullerene are clearly evident in the diffraction pattern, indicating that the hydrogenation process of this sample is homogeneous.

3.3. Scanning and transmission electron microscopy

Fig. 5 report the secondary electrons SEM pictures of the samples both as prepared and after hydrogenation at different magnifications. As-prepared $Li_6Pt_{0.11}C_{60}$ and $Li_6Pd_{0.07}C_{60}$ (a, c) powders are composed by aggregates of very different size distribution, in the range 5–60 μm, made in turn of particles also smaller than 1 μm. After hydrogenation (b, d), the size of the aggregates decreases considerably, and the powder is more fragile and fine-grained. The crystallite size remains the same as in the pristine powders. The same has been observed happening in Li_6C_{60} (results not shown). Panels a and c of Fig. 6 report the backscattered electron images which show that the platinum and palladium metals are present as 1 μm or submicron granules homogenously dispersed inside the Li–C matrix in pristine samples. The dispersion is retained also after hydrogenation (panels b, d in Fig. 6).

Fig. 7 reports two Scanning Transmission Electron Microscopy (STEM) images of $Li_6Pt_{0.11}C_{60}$; we focused on this sample only because it is the most promising with respect to its hydrogen storage properties. These pictures were collected on various sample positions and confirm the presence of transition metal particles in the sample since HAADF-STEM contrast is sensitive to the atomic number (HAADF inner cutoff angle ~46 mrad). Fulleride matrix is decorated by nanometer sized platinum particles ranging from 2 nm up to hundreds of nanometers, it is therefore possible to state that the ball milling synthesis induces platinum segregation on a broad size distribution.

3.4. Discussion

As pointed out in the introduction, the systems here studied are capable of chemically binding hydrogen. Carbon, in particular, is suitable as it can be easily hydrogenated but nonetheless the C–H binding energy is quite larger than what is required for practical applications. The C_{60} molecule can be hydrogenated to more than $C_{60}H_{40}$ [22] without displaying collapsing or fragmentation [23]. Moreover ab initio calculations suggest C_{60}–H_x ($x = 36, 48$) as the most stable structures [24] among highly symmetric $C_{60}H_{12}$*n*. These considerable high values make C_{60} a good candidate as precursor material for H storage. The high binding energy issue has been recently

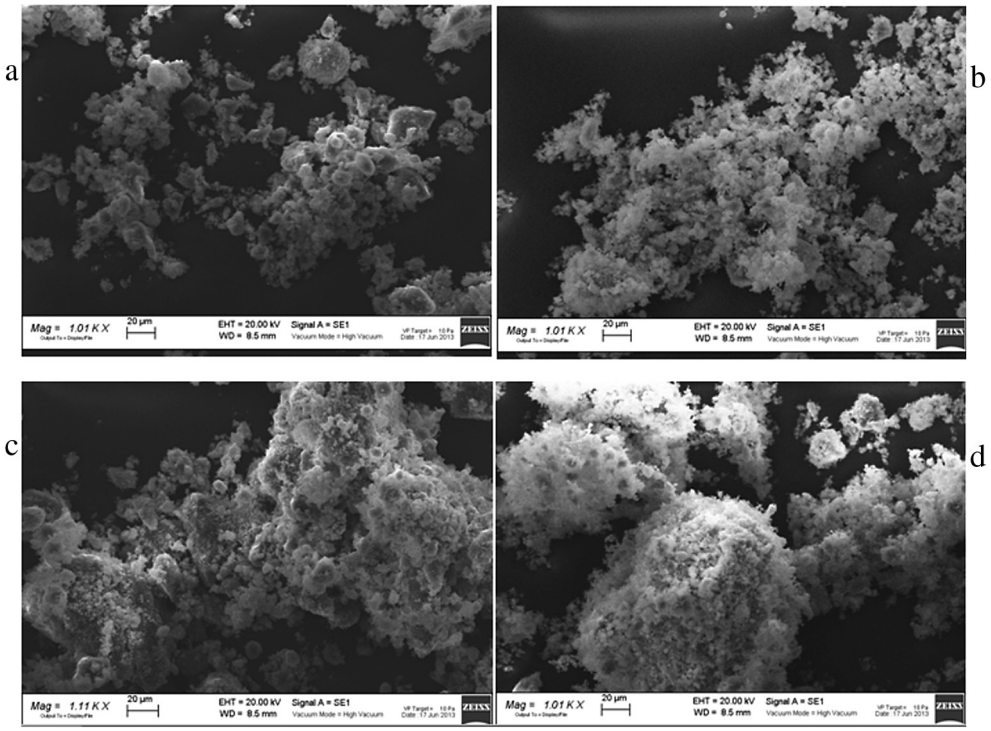

Fig. 5 – SEM secondary electrons images of pristine and hydrogenated $Li_6Pt_{0.11}C_{60}$ (a, b) and $Li_6Pd_{0.07}C_{60}$ (c, d).

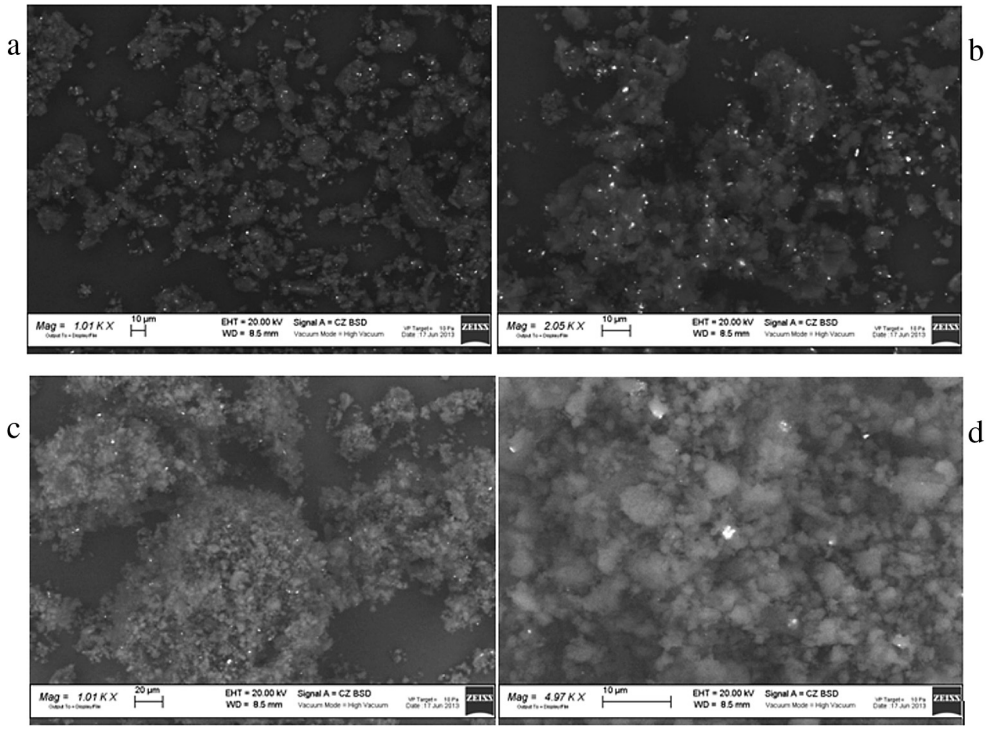

Fig. 6 – SEM backscattered electron images of $Li_6Pt_{0.11}C_{60}$ and $Li_6Pd_{0.07}C_{60}$ in pristine conditions (a, c respectively) and after hydrogenation (b, d).

overcome [11,12] by the observation that the intercalation of light, partially ionized, alkali clusters (Li, Na) in the fullerene lattice dramatically decreases the C–H binding energy, probably thanks to the highly charged state of C_{60}. The same clusters are found to mediate the H_2 molecule dissociation, so that the sum of the two processes could be considered as an alkali induced reversible "spill-over" effect [25] on C_{60} [12]. Moreover, we also observed the formation of an intermediate alkali metal hydride phase which is shown by X-ray diffraction in the hydrogen loaded material, when the alkali stoichiometry is larger than 6 [12]. This effect is absent in our case, in which no segregation is observed.

These two processes (H_2 dissociation and H chemical absorption) can be probed separately in a μSR (Muon Spin Relaxation) experiment, in which the implanted positive muons capture an electron and form muonium (a light isotope of hydrogen) [26]. The reaction of the free muonium (fully equivalent to an H atom) can then be followed by probing the muon spin evolution. In a recent μSR experiment [14] we showed that muonium gets bonded to C_{60} with a relatively

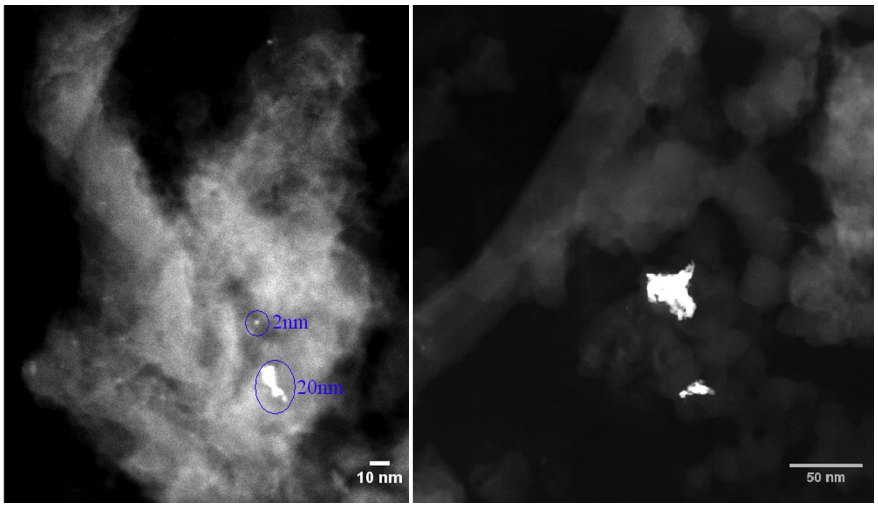

Fig. 7 – HAADF-STEM images in different sample positions and at various magnifications of $Li_6Pt_{0.11}C_{60}$ in pristine conditions.

good efficiency which, moreover, further increases at lower temperature. On the other hand, the relatively high temperatures (250 °C) required to achieve the hydrogenation of these compounds, are therefore necessary for the alkali mediated dissociation of the H_2 molecule. It was therefore proved that improving the latter process would result as an overall improvement of the sorption capabilities of these systems.

The co-intercalation of transition metals (TM) like Pt and Pd, is expected to be promoting the H_2 molecule dissociation because of the known catalytic activity on platinum and palladium surface [27,28]. This prediction is indeed confirmed by the results presented in this work.

Although the synthesis of $Li_6TM_xC_{60}$ (TM = Pt, Pd) started from a homogeneous Li–TM alloy, the high cohesion energy of TM induced its segregation into dispersed particles which are indeed still active in enhancing the H_2 dissociation. In order to demonstrate that this enhancement is ascribed to the TM catalytic activity and not to the simple hydrogenation of the TM we should exclude the formation of TM hydride in our hydrogenated samples. The platinum hydride to be formed needs indeed much higher pressure (27 GPa) than the one applied during manometric measurements [29]. Also the presence of ternary hydrides may be ruled out in $Li_6Pt_{0.11}C_{60}$ since no diffraction peaks which belong to any of their hexagonal phases may be detected in patterns presented in Fig. 3 [30,31].

A different situation is met in the case of palladium. The formation of palladium hydride [32] which does not need extreme pressure conditions like Pt, may be obtained upon hydrogenation (different hydrogen concentrations $x = 0.65$ [33], $x = 0.74$ [34] are reported in the literature). However no signature from x-ray is given for the presence of such a phase (see Fig. 4). Furthermore no diffraction due to palladium related compounds can be found in the hydrogen treated $Li_6Pd_{0.07}C_{60}$–H_{47}.

The noticeable increase of 18% (16%) in hydrogen absorption in $Li_6Pt_{0.11}C_{60}$ ($Li_6Pd_{0.07}C_{60}$) is thus attributed to the catalytic effect of TM active centers. In these systems two mechanisms are effective: alkali mediated and TM mediated dissociation. Since the reversible hydrogenation of the C_{60}^{n-} results to be much more favored with respect to the neutral molecule, we think that a further improvement in the H_2 dissociation rate would result in a further overall increase of the reversible storage capabilities of these systems. To this aim the intercalation of different TM and the synthesis using different precursors is now in progress.

4. Conclusion

The ball-milling mediated solid state reaction between fullerene and lithium-transition metals alloy is reported and it is here demonstrated to create a lithium intercalated fulleride in which a dispersion of platinum or palladium particles and/or aggregates is obtained. Hydrogenation and de-hydrogenation properties have been investigated: $Li_6Pt_{0.11}C_{60}$ and $Li_6Pd_{0.07}C_{60}$ reach a hydrogen charge value of 3 wt% and 4 wt% at 295 °C and 345 °C respectively, with a final gravimetric density around 5.9 wt% (which increases by 18% the absorption value of the solely intercalated alkali-metal fulleride) and the sorption rate results increased thanks to the transition metal catalytic activity. X-rays diffraction shows the formation of the hydrofulleride C_{60}–H_y indicating the chemisorption on fullerene molecules as the main storage process which takes place in these systems on H_2 absorption.

The proximity of the absorption values to the US-DoE 2015 goals and the scalability of the preparation process make these materials promising candidate for large scale application.

Acknowledgments

This work received financial support by the SNSF Synergia "HyCarBo" Project under the contract number CRSII2_130509/1.

REFERENCES

[1] Schlapbach L, Züttel A. Hydrogen-storage materials for mobile applications. Nature 2001;414:353–8.
[2] U.S DOE Annual energy outlook. Available online at http://www.eia.doe.gov/oiaf/aeo/.
[3] Yang S, Gao P, Bao D, Chen Y, Wang L, Yang P, et al. Mechanical ball-milling preparation of mass sandwich-like cobalt–graphene nanocomposites with high electrochemical hydrogen storage ability. J Mater Chem A 2013;1:6731–6.
[4] Fang B, Zhou H, Honma I. Ordered porous carbon with tailored pore size for electrochemical hydrogen storage application. J Phys Chem B 2006;110:4875–80.
[5] Gaboardi M, Bliersbach A, Bertoni G, Aramini M, Vlahopoulou G, Pontiroli D, et al. Decoration of graphene with nickel nanoparticles: study of the interaction with hydrogen. J Mater Chem A 2014;2:1039–346.
[6] Cabo M, Garroni S, Pellicer E, Milanese C, Girella A, Marini A, et al. Hydrogen sorption performance of MgH_2 doped with mesoporous nickel- and cobalt-based oxides. Int J Hydrogen Energy 2011;36:5400–10.
[7] Boudart M. Catalysis by supported metals. Adv Catal Relat Subj 1969;20:153–66.
[8] Kubas GJ. Metal-dihydrogen and sigma-bond coordination: the consummate extension of the Dewar–Chatt–Duncanson model for metal-olefin pi bonding. J Org Chem 2001;635:37–68.
[9] Chandrakumar KRS, Gosch SK. Alkali-metal-induced enhancement of hydrogen adsorption in C60 fullerene: an ab initio study. Nano Lett 2008;8.
[10] Sun Q, Jena P, Wang Q, Marquez M. First-principles study of hydrogen storage on $Li_{12}C_{60}$. J Am Chem Soc 2006;128:9741–5.
[11] Teprovich JA, Wellons MS, Lascola R, Hwang S, Ward PA, Compton RN, et al. Synthesis and characterization of a lithium-doped fullerane (Li_x–C_{60}–H_y) for reversible hydrogen storage. Nano Lett 2012;12:582–9.
[12] Mauron P, Remhof A, Bliersbach A, Borgschulte A, Züttel A, Sheptyakov D, et al. Reversible hydrogen absorption in sodium intercalated fullerenes. Int J Hydrogen Energy 2012;37:14307–14.
[13] Mauron P, Gaboardi M, Bliersbach A, Remhof A, Schlapback L, Zuttel A, et al. Hydrogen absorption in $Li_{12}C_{60}$. J Phys Chem C 2013;117:22598–602.
[14] Aramini M, Gaboardi M, Vlahopoulou G, Pontiroli D, Cavallari C, Milanese C, et al. Muon spin relaxation reveals the hydrogen storage mechanism in light alkali metal fullerides. Carbon 2014;67:92–7.

[15] Singh AK, Ribas MA, Yakobson BI. H-spillover through the catalyst saturation: an ab initio thermodynamics study. ACS Nano 2008;3:1657–62.
[16] Moffatt WG. The handbook of binary phase diagrams, vol. 1–2; 1976.
[17] Ricco M, Belli M, Mazzani M, Pontiroli D, Quintavalle D, Janossy A, et al. Superionic conductivity in the Li_{4}C_{60} fulleride polymer. Phys Rev Lett 2009;102:145901.
[18] Paschos O, Choi P, Efstathiadis H, Haldar P. Synthesis of platinum nanoparticles by aerosol assisted deposition method. Thin Solid Films 2008;516:3796–801.
[19] Langford JI, Wilson AJC. Scherrer after sixty years: a survey and some new results in the determination of crystallite size. J Appl Crystallogr 1978;11:102–13.
[20] Molodets AM, Lobach AS, Zhukov AN, Shulga YM, Fortov VE. Stability of crystalline structure and molecules of hydrofullerene $C_{60}H_{36}$ under high shock pressures. Doklady Phys 2008;53:562–5.
[21] Riccò M, Belli M, Pontiroli D, Mazzani M, Shiroka T, Arčon D, et al. Recovering metallicity in A_4C_{60}: the case of monomeric Li_4C_{60}. Phys Rev B 2007;75:081401.
[22] Talyzin AV. Fulleranes by direct reaction with hydrogen gas at elevated conditions. Carbon Mat Chem Phys 2010;2:85–103.
[23] Talyzin AV, Shulga YM, Jacob A. Comparative study of hydrofullerides $C_{60}H_x$ synthesized by direct and catalytic hydrogenation. Appl Phys A 2004;78:1005–10.
[24] Guo T, Scuseria GE. Ab initio calculations of tetrahedral hydrogenated buckminsterfullerene. Chem Phys Lett 1992;191:527–32.
[25] Lueking AD, Yang RT. Hydrogen spillover to enhance hydrogen storage-study of the effect of carbon physicochemical properties. Appl Catal A 2004;265:259–68.
[26] Cox SFJ. Muonium as a model for interstitial hydrogen in the semiconducting and semimetallic elements. Rep Prog Phys 2009;72:116501.
[27] Eberhardt W, Louie SG, Plummer EW. Interaction of hydrogen with a Pd(111) surface. Phys Rev B 1983;28:465–77.
[28] Eberhardt W, Greuter F, Plummer EW. Bonding of H to Ni, Pd, and Pt surfaces. Phys Rev Lett 1981;46:1085–8.
[29] Scheler T, Degtyareva O, Marquès M, Guillaume CL, Proctor JE, Evans S, et al. Synthesis and properties of platinum hydride. Phys Rev B 2011;83:214106.
[30] Bronger W. Synthesis and structure of new metal hydrides. J Alloys Compd 1995;229:1–9.
[31] Bronger W, Brassard LA. $Li_5Pt_2H_9$, a complex hydride containing isolated [Pt2H9]5- ions. Angew Chem Inr Ed EngI 1995;34:898–900.
[32] Semiletov SA, Hodyrev YuP, Baranova RV, Imamov RM. Crystal structure of palladium hydride with primitive cubic lattice. Kristallografiya 1980;25:1290.
[33] Kennedy SJ, Wut E, Kisis EH, Gray EM, Kennedya BJ. Ordering of deuterium in PdD0.65 at 54 K. J Phys Condens Matter 1995;7:L33–40.
[34] Skoskiewiz T, Baranowski B. Investigation of the electrical resistance anomaly in the palladium–hydrogen system. Phys Stat Solid 1968;30:K33–5.